JOURNAL OF GEOPHYSICAL RESEARCH, VOL. 111, B12S08, doi:10.1029/2006JB004530, 2006

Click Here for Full Article

Angular variation of the magnetic properties and reversal mode of aligned single-domain iron nanoparticles

Glenn A. Milne[1,2] and David J. Dunlop[1]

Received 26 May 2006; revised 28 July 2006; accepted 8 August 2006; published 7 November 2006.

[1] We report magnetic hysteresis and back-field demagnetization data measured at 10° intervals of the angle ψ between the applied field $\boldsymbol{H}$ and the long (magnetically easy) axes of aligned elongated single-domain iron particles electrodeposited in regularly spaced surface pores in an Al substrate. Our three samples have identical particle diameters, d = 17 nm, but varying axial ratios l/d and spacings d_c. Measured hysteresis loops resemble "hysterons" predicted by fanning, curling, and coherent rotation models of magnetization reversal, except for two features. For $\psi = 0-60°$, particle magnetizations do not reverse simultaneously at a single critical field: distributed particle coercivities produce steep but nonvertical loop segments. Broadened $\psi = 80-90°$ loops indicate imperfectly aligned particles. Comparing coercive force $H_c(\psi)$ with theoretical variations for different angular dispersions of axes and M_{rs}/M_s data with a theoretical cos ψ variation, we find a variance of 6–8.5° in particle alignment. The $H_c(\psi)$ results most closely resemble the theoretical variation for fanning rotations when $\psi \leq 50°$ and coherent rotations when $\psi > 50°$. A predicted hump in the $H_c(\psi)$ curve at intermediate angles marking the changeover from one mechanism to the other is suppressed by particle interactions (packing factors p of 0.127–0.373). Remanent coercive force measurements $H_{cr}(\psi)$ show that irreversible changes, unlike reversible rotations, are incoherent at both large and small ψ. H_{cr} continues to rise, to a high of 340–430 mT, as $\psi \rightarrow 90°$, whereas $H_c(\psi)$ decreases over the same range. $H_{cr}(\psi)$ results at large ψ favor fanning reversals for one sample and curling reversals for the other two. A Day plot of M_{rs}/M_s versus H_{cr}/H_c data gives a novel and distinctive trend from which ψ can determined within ±5° for aligned uniaxial particles.

Citation: Milne, G. A., and D. J. Dunlop (2006), Angular variation of the magnetic properties and reversal mode of aligned single-domain iron nanoparticles, *J. Geophys. Res.*, *111*, B12S08, doi:10.1029/2006JB004530.

1. Introduction

[2] Elementary hysteresis loops ("hysterons") of individual single-domain (SD) particles oriented at specific angles ψ to an applied field $\boldsymbol{H}$ are the basis of theorizing about the magnetic properties of natural dispersions of such particles in rocks, sediments and soils. Both *Néel*'s [1949] theory of thermoremanence and Preisach-first-order reversal curve (FORC) modeling of hysteresis [*Carvallo et al.*, 2005] assume hysterons that are rectangular when ψ = 0 and ramp-like when ψ = 90°. These forms in turn are based on the *Stoner and Wohlfarth* [1948] model of coherent rotation of all spins in response to $\boldsymbol{H}$ in ellipsoidal particles.

[3] It has been known since the 1950s that elongated magnetic recording particles have much lower values of coercive force H_c and remanent coercive force H_{cr} than predicted by the Stoner-Wohlfarth model. Incoherent rotation and reversal modes like curling and fanning [*Jacobs and Bean*, 1955] predict more realistic coercivities and critical fields. More recently, numerical micromagnetic modeling has shown that SD particles may reverse by a combination of quasi-coherent ("flower") and incoherent ("vortex") spin rotations [*Williams and Dunlop*, 1995; *Fabian et al.*, 1996], the latter resembling curling reversals predicted analytically.

[4] Testing these theoretical predictions has been difficult because of problems in producing experimental samples whose magnetic particles are (1) uniform in size and shape, (2) uniformly spaced, and (3) mutually aligned. One method of accomplishing this is to electrodeposit a ferromagnetic metal, usually iron, in aligned cylindrical pores in an oxidized aluminum substrate [*Pontifex et al.*, 1991]. The hysteresis [*AlMawlawi et al.*, 1991] and remanence [*Dunlop et al.*, 1993] of these particle arrays are consistent with reversal by fanning in a chain of spheres. Electron microscopy indicates that the individual iron particles do resemble chains of fused spheres [*Pontifex et al.*, 1991].

[5] The present paper extends this earlier work with detailed measurements of coercivities, critical fields, and elementary hysteresis loops as a function of field angle ψ. We also test the effect of particle interaction as inferred from

[1] Geophysics, Department of Physics, University of Toronto, Toronto, Ontario, Canada.
[2] Now at Department of Earth Sciences, University of Durham, Durham, UK.

0148-0227/06/2006JB004530$09.00

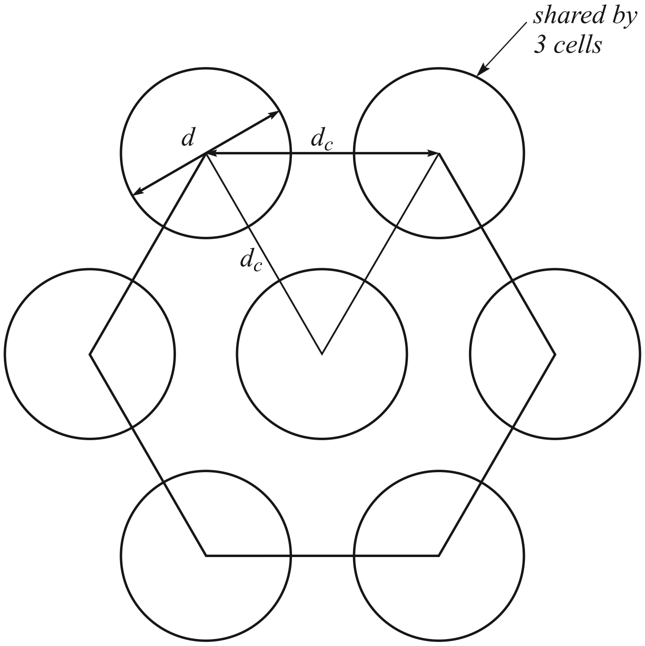

Figure 1. Schematic of pores arranged in hexagonal cells in the plane of the substrate. The pore or iron particle diameter is d, and the pore spacing or cell size is d_c. Particles/pores extend perpendicular to the plane of view for lengths $l \gg d$.

particle spacing and magnetic packing fraction. It is our intention to establish more realistic hysterons as the basis of theories of thermoremanence and the interpretation of Preisach-FORC diagrams.

2. Samples and Experimental Methods

[6] When aluminum is the anode in an electrochemical cell with an acid electrolyte, a porous oxide film forms on the surface of the aluminum. The pores are aligned perpendicular to the surface and form a honeycomb array of hexagonal cells (Figure 1). The pores are quite uniform in length, diameter d and center-to-center spacing d_c [*Furneaux et al.*, 1978]. Iron is deposited in the pores by AC electrolysis, deposition beginning at the base of each pore and proceeding upward. The length l of the iron particle is controlled by electrodeposition time. Particle density is about 90% that of a particle of pure iron with the same l and d values, suggesting either a noncylindrical shape or incorporation of some Al_2O_3 in the particle. *Pontifex et al.* [1991] report that the particle morphology is a chain of fused spheres, not a cylinder.

[7] The three samples used in this study were selected from a large series produced by anodizing the aluminum substrate in voltages from 5 to 25 V, giving a range of cell sizes d_c from 26.5 to 64.5 nm. Our samples have d_c values of 26.5, 36 and 45.5 nm, which correspond to magnetic packing factors (Fe/Al_2O_3) $p = (\pi/2\sqrt{3})\ (d/d_c)^2$ of 0.373, 0.202 and 0.127 (Table 1). Oxalic acid was used as the electrolyte, giving highly acicular pores with average aspect ratios around 20. The pore diameter d can be increased by aging in phosphoric acid but the pores in our three samples were purposely left untreated. Their iron particles have d = 17 nm, well within the stable SD range [*Kneller and Luborsky*, 1963; *Butler and Banerjee*, 1975].

[8] The fanning model of magnetization reversal [*Jacobs and Bean*, 1955] predicts a dependence of coercive force H_c on particle elongation which agrees well with experimental H_c values for the large series [*AlMawlawi et al.*, 1991]. H_c is a strong function of l/d for small aspect ratios but H_c is virtually constant when $l/d \geq 10$, which is the case for our samples 14, 34 and 96. In order to match the absolute values of H_c, *AlMawlawi et al.* [1991] assumed a saturation magnetization M_s = 1305 kA/m, ≈25% lower than M_s = 1715 kA/m for pure iron. This seems unreasonably low; we tentatively use a value M_s = 1500 kA/m based on the measured density.

[9] Hysteresis curves were measured using a Princeton Applied Research vibrating sample magnetometer (VSM). Hysteresis loops closed in fields of 0.5–0.6 T. The negative diamagnetic signal of the Al and Al_2O_3 substrate, most evident between 0.6 and 1 T, was removed from the entire loop. Each 10 mm × 15 mm sample (cut from the oxidized Al sheet) was mounted with its plane vertical in a Plexiglas holder which could be rotated about the vertical. Ten hysteresis loops were measured for field angles ψ = 0 (i.e., $\boldsymbol{H}$ perpendicular to the sheet), 10°, 20°, . . ., 90° ($\boldsymbol{H}$ in the plane of the sheet), with an accuracy of approximately ±0.5°. The hysteresis parameters H_c and M_{rs} (saturation remanence) were determined directly from the measured loops. Remanent coercive force H_{cr} was determined by removing samples in their saturation remanence state and measuring back-field demagnetization curves with a Digico spinner magnetometer.

3. Theoretical Background

[10] Numerical micromagnetic modeling has not yet been carried out systematically enough to predict elementary hysteresis loops at an arbitrary field angle ψ. We therefore concentrate on analytical modeling. *Brown* [1963] derived a set of nonlinear differential equations specifying the magnetic energy as a function of field $\boldsymbol{H}$ and the angles between the magnetization $\boldsymbol{M}$ and the easy axes of anisotropy. In principle, the hysteresis curve of a particle is obtainable by solving Brown's equations but the problem is only tractable by making a number of simplifying assumptions. If $\boldsymbol{H}$ is large enough that $\boldsymbol{M}$ is saturated (all spins aligned), the equations can be linearized. In reducing and reversing the field, a point will be reached where the uniform $\boldsymbol{M}$ state is no longer energetically favored and transforms, usually abruptly and discontinuously, into a nonuniform state. At the nucleation field H_n where this occurs, nonuniformity is small enough that linearization is still valid. Generally H_n is equal to the critical field H_{crit} for reversal of $\boldsymbol{M}$.

Table 1. Dimensions d and l, Spacing d_c, and Packing Fraction p of Iron Particles in the Experimental Samples

Sample	d, nm	l/d	d_c, nm	p
14	17	19	26.5	0.373
34	17	14	36	0.202
96	17	40	45.5	0.127

[11] The assumption of uniform $\boldsymbol{M}$ is only valid for ellipsoidal particles or within individual particles in an interacting array, e.g., a chain of spheres that touch but have no exchange interaction. In a prolate spheroid, *Aharoni* [1963] found three reversal modes: coherent rotation for small d, curling (a propagating vortex/circular spin configuration) for large d, and possibly buckling (a wave-like deviation of spins from the long axis) in a narrow range of intermediate d. In a chain of spheres, *Jacobs and Bean* [1955] reported two modes: coherent rotation with critical fields about one half those of a spheroid of the same l/d, and for larger d a buckling-like mode called fanning.

[12] In *Jacobs and Bean*'s [1955] model, $\boldsymbol{H}$ is along $-z$ and $\boldsymbol{M}$ is initially positive and along the chain axis, which is in the x-z plane at angle ψ to $+z$. The chain contains n spheres, so the aspect ratio $l/d = n$. When $\boldsymbol{M}$ deviates from the chain axis in response to increasingly negative $\boldsymbol{H}$, $\boldsymbol{M}$ remains uniform within each sphere. In fanning, the moment $\boldsymbol{\mu} = (\pi/6)d^3\boldsymbol{M}_\mathbf{s}$ of alternate spheres is at alternating angles $\pm\theta$ to $+z$ (in contrast to coherent rotation, where $\boldsymbol{\mu}$ is at the same polar angle θ for all spheres) and at azimuthal angle ϕ to $+x$. In symmetric fanning, ϕ is constrained to have a constant magnitude but opposite sign in neighboring spheres. Nonsymmetric (unconstrained) fanning has lower critical fields but is much more difficult to solve for.

[13] For a prolate spheroid, *Stoner and Wohlfarth* [1948] considered two energies: $E_\mathrm{H} = -\boldsymbol{\mu} \cdot \boldsymbol{H}$ and the angle-dependent demagnetizing energy E_d. Spheres have no shape anisotropy but magnetostatic interaction among the spheres, described by *Jacobs and Bean* [1955] in terms of the dipole-dipole energy, produces an equivalent anisotropy with the easy axis along the chain (the dipole moments $\boldsymbol{\mu}$ tend to line up in the absence of $\boldsymbol{H}$). Minimizing the sum $E_\mathrm{H} + E_\mathrm{ms}$, they found possible solutions

$$\phi = 0,\ \pi \tag{1a}$$

or

$$\cos\phi = A(n, \psi)\cot\theta, \tag{1b}$$

where $A(n, \psi)$ is a combination of numerical coefficients depending on n and sin and cos of ψ. The first two solutions, $\phi = 0, \pi$, represent coherent rotation and the third is fanning. The initial deviation from the easy axis is always coherent rotation (all sphere moments $\boldsymbol{\mu}$ parallel), with a discontinuous change to a fanning reversal at $\theta = \tan^{-1} A(n, \psi)$. With increasing field angle ψ, the range of θ for which fanning occurs narrows and ultimately disappears around 50–55° depending on n. Thus fanning occurs when a field is applied at a small angle to the chain and coherent rotation takes over at larger angles.

[14] The third possible mode of reversal in a chain of spheres is curling. *Aharoni* [1966] calculated for $\psi = 0$

$$H_\mathrm{n} = 0.335 - 1.379S^{-2} \tag{2}$$

where $S = (M_s d/2)\,(C/2)^{-1/2}$, C being the exchange constant. Exchange energy is involved because $\boldsymbol{M}$ is no longer uniform within a sphere. Using second-order perturbation theory, Aharoni extended his calculation to a general angle ψ, for which the result for H_n is considerably more intricate. As for the fanning calculation, the initial response to $-\boldsymbol{H}$ is a reversible parallel rotation of all sphere moments up to a critical angle θ, marking H_n, at which there is a sudden onset of curling and $\boldsymbol{M}$ reverses. Also in common with fanning, curling occurs for small and intermediate field angles, above which changes in $\boldsymbol{M}$ occur by coherent rotation.

[15] For $S < 1.634$, fanning has a lower H_n than curling. Thus, as for spheroids, the reversal modes for small, intermediate and large d are coherent rotation, fanning and curling, respectively. The transition sizes depend on the material properties M_s and C. Even for larger sizes, reversals become coherent above a critical value of ψ.

[16] When $\psi > 45°$, $\boldsymbol{M}$ rotates reversibly through a large enough angle θ that the magnetization M measured in the direction of $\boldsymbol{H}$ becomes zero at a field smaller than the critical field H_crit. The field for which $M = 0$ (but from which $\boldsymbol{M}$ may return to its original orientation if $\boldsymbol{H}$ is reduced or removed) is the coercive force H_c. The critical field at which $\boldsymbol{M}$ rotates irreversibly is measured experimentally as the remanent coercive force H_{cr}. The dependences of H_c and H_{cr} on ψ are identical for $\psi \leq 45°$ but very different for $\psi > 45°$, as will be evident in figures later in the paper where the solutions of (1), (2), and the generalization of (2) are plotted.

4. Experimental Results

[17] Representative hysteresis loops for sample 96, at ψ = 0, 30°, 60°, 80° and 90°, are plotted in Figure 2 and compared with theoretical loops calculated for coherent rotation (short dashes) and fanning (long dashes). Experimental M_{rs}/M_s, H_c, H_{cr}, and H_{cr}/H_c results for all samples as a function of ψ appear in Table 2.

[18] A number of features are immediately apparent from the loops. For small field angles, the critical field predicted by the *Stoner and Wohlfarth* [1948] coherent rotation model is much higher than H_c observed experimentally. The same is true for refinements of the Stoner-Wohlfarth model [e.g., *Fulmek and Hauser*, 1994]. A closer match is that of the fanning model, which predicts almost the correct H_c and reversal field values over the range $0 \leq \psi \leq 50°$. Small differences between observed H_c and fanning predictions may result from thermal agitation, which can overcome the small energy barriers near the switching field. The difference between the axis-crossing field H_c and the critical field H_crit for reversal (vertical loop segment) is apparent in the theoretical 60° and 80° loops.

[19] The samples fall some way short of the ideal of perfectly aligned particles of identical size and elongation. A distribution of d and/or l/d, and hence of coercivities, is evident in Figures 2a and 2b, where the irreversible part of the measured loop is steep but far from vertical, in contrast to theoretical loops for coherent rotation, fanning, and a curling-type nucleation in a rectangular grain with $\psi \approx 27°$. A distribution of particle axis orientations affects all the loops, most clearly in the ψ = 90° data which should theoretically follow a reversible ramp but in practice are irreversible, with a hysteresis loop about half as wide as the ψ = 80° loop.

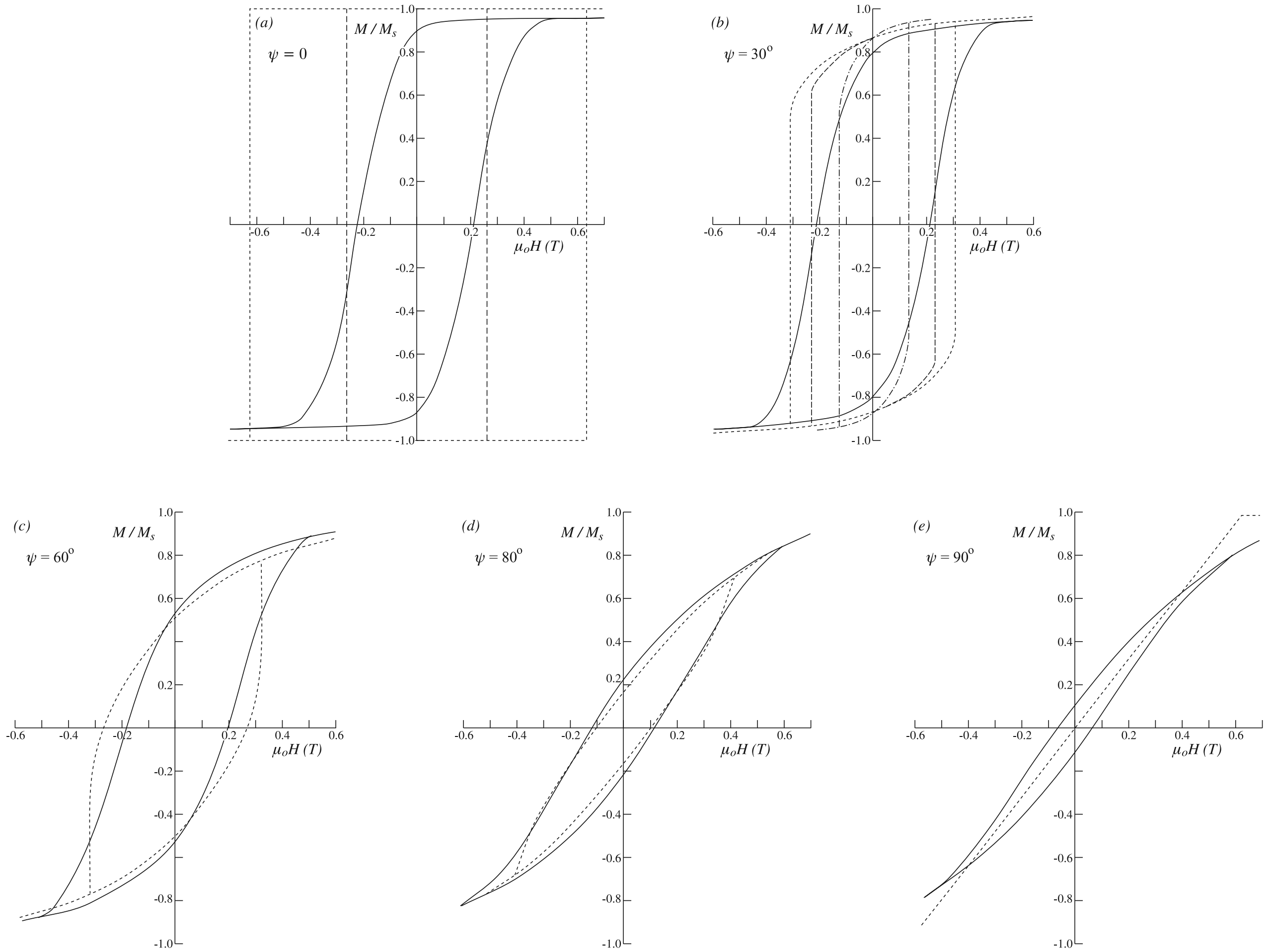

Figure 2. Selected experimental hysteresis loops for sample 96 (solid curves) at field angles ψ from 0 (***H*** applied perpendicular to the substrate, parallel to particle axes) to 90° (***H*** in the plane of the substrate, perpendicular to particle axes). Theoretical hysterons are for coherent rotation (short dashes), symmetric fanning (long dashes), and curling in a rectangular prism of magnetite with l = 74 nm, l/d = 1.5, $\psi \approx 27°$, rescaled for iron (Figure 2b, dot-dashed [*Newell and Merrill*, 2000]).

[20] In Figure 3, values of H_c for all three samples are compared to $H_c(\psi)$ as predicted by curling, fanning and coherent rotation models. Note that when $S \leq 1.634$, fanning is a lower-energy mode than curling, and that coherent rotation becomes the preferred mode when $\psi >$ 50°, 60° or 70° for S = 1.634, 1.8 or 2.0, respectively. When ***H*** is applied close to the chain axis, H_c is far below *Stoner and Wohlfarth*'s [1948] and *Jacobs and Bean*'s [1955] predictions for coherent rotation (see also Figure 2a). As ψ increases, H_c decreases slightly rather than increasing as predicted by fanning and curling models. The predicted peak in H_c at intermediate ψ is present only in sample 14 and occurs around ψ = 65°, implying curling rather than fanning reversals at lower ψ.

Table 2. Hysteresis Properties of the Experimental Samples

	Sample 14				Sample 34				Sample 96			
ψ, deg	M_{rs}/M_s	H_c, mT	H_{cr}, mT	H_{cr}/H_c	M_{rs}/M_s	H_c, mT	H_{cr}, mT	H_{cr}/H_c	M_{rs}/M_s	H_c, mT	H_{cr}, mT	H_{cr}/H_c
0	0.983	212	221	1.04	0.870	221	241	1.09	0.928	216	226	1.05
10	0.982	210	218	1.04	0.868	219	232	1.06	0.918	216	228	1.05
20	0.962	204	216	1.06	0.863	212	230	1.09	0.900	210	225	1.07
30	0.916	199	212	1.07	0.821	204	227	1.12	0.858	205	226	1.10
40	0.855	197	218	1.11	0.782	196	229	1.17	0.795	201	231	1.15
50	0.753	198	229	1.16	0.695	189	237	1.26	0.703	198	244	1.23
60	0.630	200	249	1.25	0.563	177	252	1.42	0.566	191	267	1.40
70	0.485	194	276	1.42	0.395	152	274	1.80	0.403	171	298	1.74
80	0.265	147	349	2.37	0.225	96.4	298	3.09	0.227	116	349	3.00
90	0.078	88.4	432	4.88	0.138	60.2	336	5.58	0.115	63.9	373	5.83

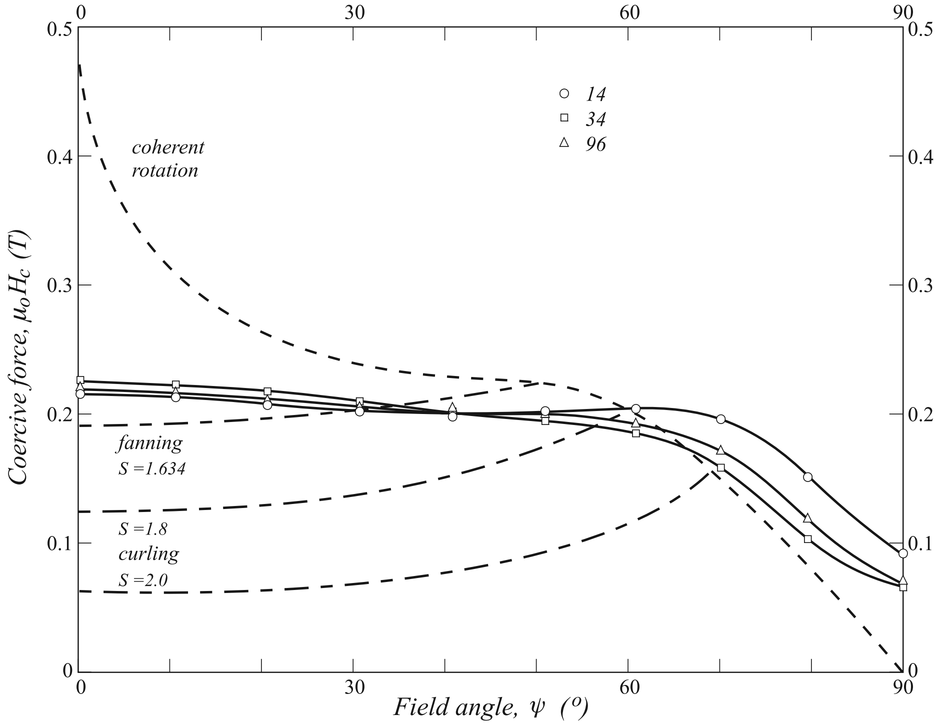

Figure 3. Coercive force data for all samples as a function of field angle ψ, compared with model predictions for coherent rotation, symmetric fanning, and curling in an infinite chain of spheres. $S = (M_s d/2)(C/2)^{-1/2}$ is reduced particle diameter. Fanning is energetically preferred over curling when $S \leq 1.634$. Coherent rotation is preferred over fanning or curling when $\psi > 50$–$70°$, leading to a predicted $H_c(\psi)$ that peaks at intermediate angles. The experimental $H_c(\psi)$ results do not rise to a peak; they are nearly constant at small ψ and decrease rapidly above $\psi = 70°$.

[21] In theory a chain of spheres reverses its magnetization at a field H_{crit} identical to the axis-crossing field H_c if $\psi \leq 45°$. When $\psi > 45°$, $\boldsymbol{M}$ must be rotated past $M = 0$ before it switches irreversibly, so that $H_{\mathrm{crit}} > H_c$. Thus the theoretical curves are the same in the left halves of Figures 3 and 4 but quite different in the right halves, H_{crit} increasing with increasing ψ for all models. However, there is an experimental problem in testing these predictions. In theoretical loops, the reversal is recognizable as a vertical discontinuity in $\boldsymbol{M}$ but measured loops never have such jumps because there is always a distribution of microcoercivities. Therefore we use H_{cr} from back-field demagnetization as a measure of average microcoercivity or switching field. The H_{cr} data have the general aspect of the variations predicted by fanning and curling models, although the data for samples 34 and 96 do not rise as steeply as predicted at large ψ.

[22] All theoretical curves assume that ψ is the same for each particle, i.e., that the chains are all mutually aligned perpendicular to the substrate surface. In reality there is a dispersion in orientation and this affects both H_c and M_{rs}/M_s data. The effect is most noticeable for $\psi = 90°$: we measure $H_c = 60$–90 mT and $M_{rs}/M_s = 0.08$–0.14, whereas both are predicted to be zero. Figure 5 shows the effect of assuming a normal distribution of particle alignment with a variance of 8.5° on $H_c(\psi)$ for fanning plus coherent rotation and compares this theoretical curve with the measured $H_c(\psi)$ data. There is an approximate fit for $\psi \geq 60°$, where H_c is most affected by angular dispersion. An independent estimate, using the fact that for an aligned array $M_{rs}/M_s(\psi) = \cos\psi$, is $\cos^{-1}[M_{rs}/M_s(90°)]$ which gives a mean of 83.7° instead of the ideal 90°.

[23] The parameters M_{rs}/M_s and H_{cr}/H_c are indicators of domain structure among other things. High values of one parameter correspond to low values of the other but a richer source of information comes from utilizing both simultaneously in a plot of M_{rs}/M_s versus H_{cr}/H_c (a *Day et al.* [1977] plot). Day plot curves vary considerably depending on the magnetic mineral(s) involved, the fineness of particle size (superparamagnetic grains, for example, give distinctive curves entirely unlike those of coarser grains), and particle interactions [*Dunlop*, 2002a, 2002b; *Dunlop and Carter-Stiglitz*, 2006]. The data for our (almost) aligned particles (Figure 6) add a new mineral, iron, and a new parameter, field angle ψ, to those considered previously. The trend for iron nanoparticles as ψ increases lies above and to the right of the trend for PSD magnetites as grain size increases (100 nm to 20 μm [*Dunlop*, 2002a, Figure 2]). Since randomly oriented particles are the norm in nature, there is no likelihood of any ambiguity for real rock data.

5. Discussion

5.1. Angular Dispersion and Elementary Hysteresis Loops

[24] A major objective of our work was to produce a set of basis hysterons for uniaxial SD particles at 10° increments of field angle ψ. The *Néel* [1949] theory sidesteps the issue of angular dispersion by replacing real ensembles of

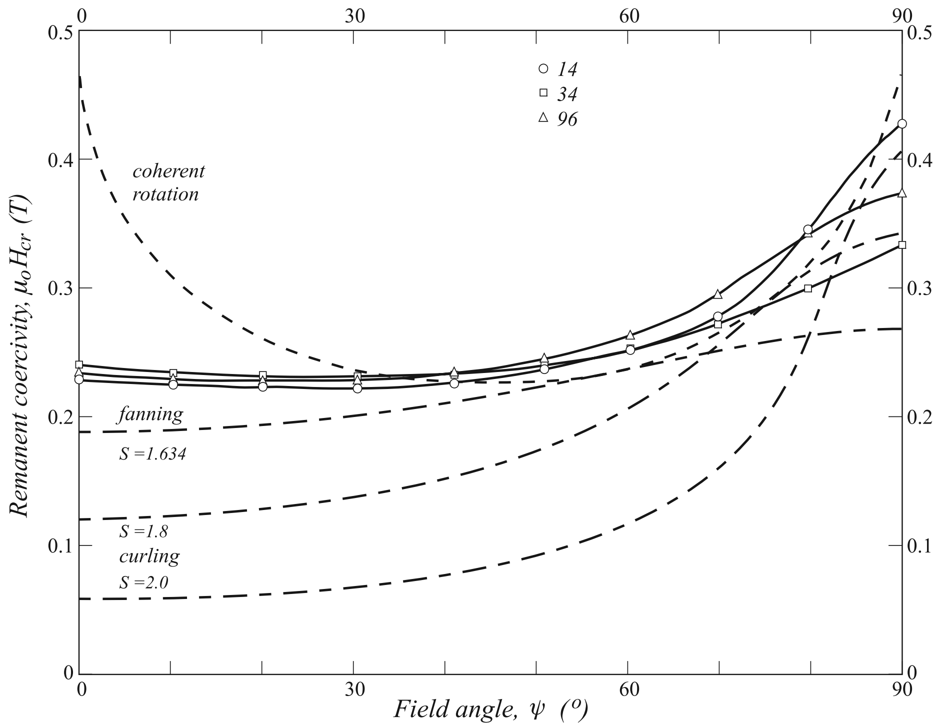

Figure 4. Measured remanent coercive force $H_{cr}(\psi)$ for all samples, compared with coherent rotation, symmetric fanning, and curling predictions. On the left side, theoretical curves are identical to those in Figure 3 because $\boldsymbol{M}$ reverses at H_c. However, when $\psi > 45°$, reversal occurs at a critical field $H_{\mathrm{crit}} > H_c$ and the fanning and curling curves continue to climb, meeting the coherent rotation curve tangentially (fanning, curling with $S = 1.8$) or not at all (curling, $S = 2.0$). The data follow the fanning curve except at $\psi \geq 70°$, where the experimental curves climb and diverge.

randomly oriented particles by an artificial distribution in which one third of the particles are aligned parallel to $\boldsymbol{H}$ and have rectangular hysteresis loops while the other two thirds are perpendicular to $\boldsymbol{H}$ and have reversible ramp-like magnetization curves. While this approximation results in the correct value for initial susceptibility, the actual $M_{rs}/M_s = 0.5$ is 50% higher than the predicted 0.333. The effect on TRM of particle ensembles has never been studied in detail (see, however, *Egli and Lowrie* [2002] and *Lanci and Kent* [2003]). The *Preisach* [1935] phenomenology and FORC analysis based on it use the same simplified hysterons to represent irreversible and reversible processes, respectively.

[25] The Preisach-Néel approximations are not necessary. *Stoner and Wohlfarth*'s [1948] theory generates hysterons at any ψ (shown in Figures 2a–2e) which could be introduced numerically in *Néel*'s [1949] theory. The problem is that coherent rotation is not the lowest-energy mode when ψ is small. Depending on particle size and morphology, either curling or fanning is preferred. Theoretically coherent rotation only becomes energetically favorable compared to fanning when $\psi > 50°$ (Figure 3) and the angles are even larger for curling. In fact, the theoretical curves in Figure 4 imply that when irreversible switching at $\psi > 45°$ is involved (i.e., a critical field rather than a coercive force H_c), fanning or curling take over from coherent rotation as the preferred mode at large as well as small ψ. Magnetic recording research has concentrated on $H_c(\psi)$ but $H_{\mathrm{crit}}(\psi)$ (as measured by $H_{cr}(\psi)$, for example) is more significant in rock magnetism, where the remanence carried by a rock and switching between remanent states are of paramount importance.

[26] A complete set of hysterons for arbitrary ψ is more challenging to compute for fanning and curling than for coherent rotation. Furthermore we have little information about which process, fanning or curling, is preferred in practice. Hence experimental hysteresis loops like the ones we have measured (e.g., Figures 2a–2e) are of great potential value. Unfortunately, even our well-controlled samples do not contain perfectly aligned particles. On the basis of the average value $M_{rs}/M_s \approx 0.11$ for the three samples when $\psi = 90°$, the pores into which the iron particles were deposited are at an average angle of $\approx$84° to the substrate surface rather than the ideal 90°. A similar estimate of misalignment, 8.5°, comes from measured H_c values at $\psi = 90°$. This angular dispersion is of similar magnitude to the desired increment in ψ of 10° between basis hysterons.

[27] The problem is well illustrated by comparing Figures 2d and 2e. The experimental $\psi = 90°$ loop is >100 mT wide where it crosses the field axis and resembles a scaled-down version of the $\psi = 80°$ loop. Each of the experimental loops is an average of loops at a distribution of angles and is therefore broadened and smoothed compared to the theoretical functions. The effect is most pronounced at large ψ where the loops change shape most rapidly with changing field angle.

[28] To obtain "experimental" loops without angle averaging, we need to perform an inversion. We have been

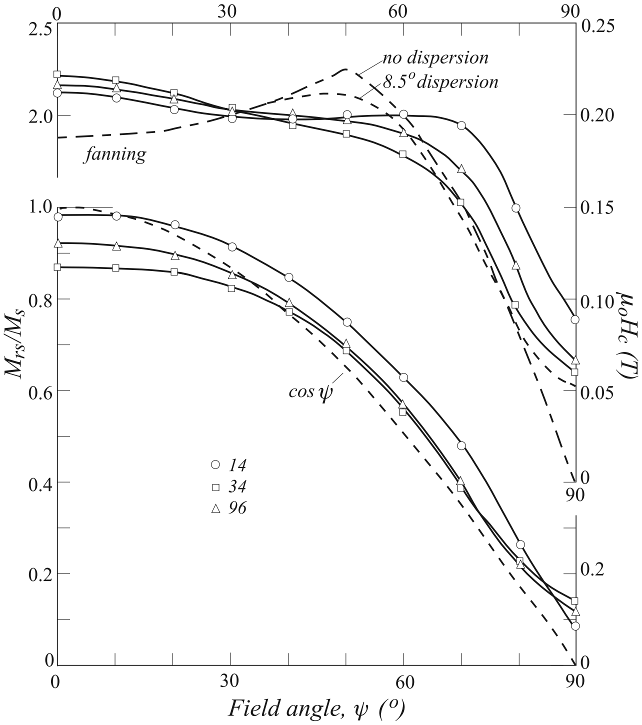

Figure 5. Effect of angular dispersion of particle axes illustrated by experimental and theoretical $H_c(\psi)$ and $M_{rs}/M_s(\psi)$ curves. An average 8.5° dispersion produces best fit of the fanning curve to $H_c(\psi)$ data from 70 to 90°. Note that H_c does not drop to zero at $\psi = 90°$ because many particles have their axes at <90° to the field. For the same reason, $M_{rs}/M_s > 0$ at $\psi = 90°$, although theoretically, $M_{rs}/M_s(\psi) = \cos\psi \rightarrow 0$.

content to seek a best fit to the measured $H_c(\psi)$ data using the theoretical hysterons as basis functions and convolving them with a normal distribution of ψ with adjustable variance. The resulting fits are not impressive (Figure 5) and imply that the coherent rotation hysterons are not very close to the correct set of basis functions, even for large ψ. The rather coarse set of hysterons we used, with increments of 10° in ψ, may be part of the problem.

[29] Even if the inversion were carried out, we must confront another problem. The ideal hysterons have a single critical field at which all particles reverse their moments but it is clear in Figures 2a, 2b, and 2c that the actual loops have long inclined segments where the theoretical loops have vertical discontinuities. In other words, magnetization reversal occurs progressively over a range of critical fields: the particles are characterized by a coercivity spectrum, not a single field at which they all simultaneously switch. Only if we could produce an ideal sample having a single particle size and shape could we obtain quasi-rectangular loops. Chains of magnetosomes produced by magnetotactic bacteria come close to this ideal (see hysteresis curve MV1H in the work by *Dunlop and Carter-Stiglitz* [2006], for example) but as part of a living organism, the linearity of the chain can change [*Kobayashi et al.*, 2006], greatly reducing the coercivity [*Hendriksen et al.*, 1994]. Magnetic recording particles also have relatively narrow coercivity spectra but the alignment of their particles is typically not as good as that of our iron particles [*Luborsky and Paine*, 1960; *Knowles et al.*, 1980].

5.2. Effects of Particle Interaction

[30] One of our purposes was to examine the effects of particle interaction. Interaction strength varies among samples because of differing particle spacing or cell size d_c (Figure 1). The magnetic packing factor p (= volume of iron/total volume) ranges from 0.127 in sample 96 to 0.373 in sample 14 (Table 1). These are high packing factors and should lead to strong interchain interactions. Interactions also change as field angle ψ changes. In the remanent state or for small ψ, $\boldsymbol{M}$ lies along or close to the particle axis. In an array of side-by-side chains, the interactions are then negative: the external field $\boldsymbol{H}_{\mathbf{int}}$ produced by each particle is in the opposite direction to $\boldsymbol{\mu} = V\boldsymbol{M}_{\mathbf{s}}$ of its six nearest neighbors. For large ψ, $\boldsymbol{H}$ pulls $\boldsymbol{M}$ away from the long axis toward the plane of the substrate. Then we have a planar array of parallel lines of moments, arranged head to tail within each line. Each line interacts negatively with neighboring lines, but the interactions within a line are positive (producing the head-to-tail arrangement). A dipole field is twice as strong along the dipole axis as perpendicular to it. If the dipoles were distributed uniformly in space, the greater number of perpendicular dipoles would compensate for the weaker interaction and the overall interaction field would be zero [*Dunlop and Özdemir*, 1997, pp. 38–39]. For a uniform distribution on a plane, however, the positive interactions dominate.

[31] The difference between the theoretical $H_c(\psi)$ function for fanning or curling and $H_c(\psi)$ as measured for our samples (Figure 3) probably results from strong interactions. Theoretically, H_c increases as ψ increases from 0 and peaks at intermediate ψ (50° to 70°) when coherent rotation becomes favored, causing H_c to decrease with further increases in ψ. Experimentally, H_c is constant or decreases slightly with increases in ψ up to 60°. *Bottoni* [1991] demonstrated exactly this effect in experiments on aligned magnetic recording particles. For small p (0.01–0.02), $H_c(\psi)$ peaked at intermediate angles as predicted, but as p increased from 0.065 to 0.3, approximately the range covered by our samples, the peak flattened and evolved to a monotonically decreasing $H_c(\psi)$. *Luborsky and Paine* [1960] reported a similar trend for elongated iron particles but their range of p was more limited: 0.08, 0.35 and 0.47.

[32] We expected that changing p would have a direct effect on hysteresis. Negative interactions should lower both H_c and M_{rs}/M_s [*Luborsky and Paine*, 1960], but no such effect is evident in Table 2. Sample 14, with the largest p, has the lowest H_c but the highest M_{rs}/M_s values for ψ = 0–30°. In the range $70° \leq \psi \leq 90°$, sample 14 has the largest H_c, possibly as a result of positive interactions but M_{rs}/M_s drops to a value lower than that of the other samples at ψ = 90°. Relative values of both parameters for samples 34 and 96 are in many cases opposite to what is expected from their p values. The lack of clear trends may mean that the pores and the iron particles they contain are not as uniformly arranged as Figure 1 indicates. Because of the $1/r^3$ dependence of dipole fields, the closest neighbor in an irregular array has a disproportionate effect on the interaction field.

[33] An unexpected observation was that M_s increased monotonically by ≈30% as ψ increased from 0 to 90°. This

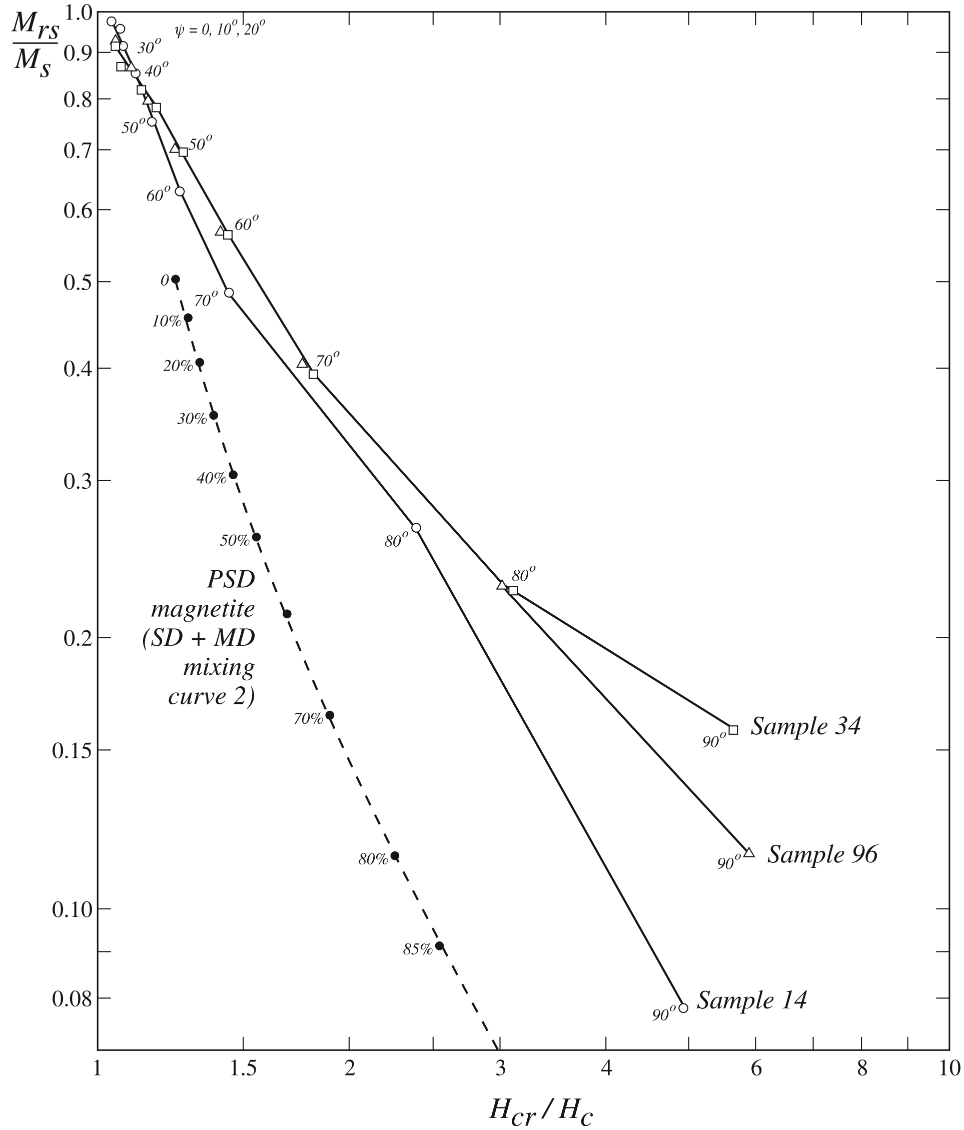

Figure 6. A Day plot of M_{rs}/M_s and H_{cr}/H_c data as a function of ψ, compared to the mixing curve for pseudosingle-domain (PSD) magnetite as a function of percent MD end-member.

is not an instrumental effect because the diamagnetic signal of the substrate remained constant. We surmise that the change from dominantly negative to net positive interactions as ψ increases is responsible but it seems implausible that saturation could be inhibited by interactions in applied fields as large as 1 T.

5.3. Reversal Modes

[34] When $\psi \leq 30°$, experimental values of H_c and H_{cr} are much lower than predicted for coherent rotation (Figures 2a, 2b, 3, and 4). They vary with ψ approximately as expected for symmetric fanning but absolute values are higher than predicted. Likely our assumed value M_s = 1500 kA/m is too low and M_s = 1715 kA/m for pure iron should be used. This would raise predicted H_c and H_{cr} values by $\approx$15%, giving a good match with H_c measured when $\psi = 0$. Observed H_{cr} values would still be $\approx$5% high, but although in theory $H_{\mathrm{crit}} = H_c$ when $\psi \leq 45°$, in practice H_{cr} is always somewhat greater than H_c.

[35] When $\psi > 45°$, predicted $H_{\mathrm{crit}}(\psi)$ and $H_c(\psi)$ dependences diverge for all models. Observations of $H_c(\psi)$ follow the predicted coherent rotation variation (Figure 3) apart from the effect of angular dispersion. The reversible magnetization changes responsible for H_c at large angles appear to occur by parallel rotation of all sphere moments. However, our experimental $H_{cr}(\psi)$ data (Figure 4) do not clearly favor one model over the others. $H_{cr}(\psi)$ for sample 34 resembles the predicted fanning variation for $\psi \geq 70°$, while $H_{cr}(\psi)$ for sample 96 in the same range resembles the curve for curling with S = 1.8. $H_{cr}(\psi)$ for sample 14 rises steeply at ψ = 80° and 90°, in the manner of the S = 2.0 curling curve.

[36] *Aharoni* [1986] gives an expression for H_{n} due to curling in tape particles:

$$H_{\mathrm{n}}(\psi)/H_{\mathrm{n}}(0) = \left(1 - \alpha \sin^2 \psi\right)^{-1/2}, \tag{3}$$

where α is related to the reduced particle radius S. Equation (3) approximately fits switching fields calculated by micromagnetic theory for 3:1 and 5:1 elongated γFe_2O_3 particles at 20° intervals of ψ [*Schabes and Bertram*, 1988], the distribution $H_{crit}(\psi)$ of critical fields of 30 nm and 70 nm diameter elongated iron particles measured by magnetic force microscopy [*Luo and Zhu*, 1994], and the angular dependence (measured at 15° intervals of ψ) of median destructive field (AF demagnetization) of anisotropic dispersions of 0.7–82 μm magnetite particles [*Stephenson and Shao*, 1994]. Equation (3) is a less satisfactory description of our $H_{cr}(\psi)$ results, in part because our H_{cr} values decrease from ψ = 0 to 30° but more importantly because of the diverse curve shapes when $H_{crit}(\psi) \geq 70°$.

[37] From equation (2), $S = (M_s d/2)\ (C/2)^{-1/2}$. The calculation must be done in cgs units. Substituting M_s = 1715 emu/cm^3, $d = 1.7 \times 10^{-6}$ cm and $C = 4.0 \times 10^{-6}$ erg/cm gives S = 1.03. Any value of S < 1.634 implies fanning rather than curling reversal. On these purely theoretical grounds, the iron particles would have to have diameters of at least 27 nm before curling reversals would be favored.

[38] However, our iron particles consist of fused quasi-spherical crystallites rather than separate (i.e., nonexchange-coupled) spheres. Their behavior could be more akin to that of long cylinders or ellipsoids. *Aharoni and Shtrikman* [1958] concluded that curling was favored in an infinite cylinder if S > 1.08. For smaller radii, there was only a narrow range of S in which buckling, the analog of symmetric fanning, was favored over coherent rotation. For prolate spheroids, *Aharoni* [1963] found that buckling was a marginal mode, and *Aharoni* [1997] eliminated it entirely. The critical reduced radius above which curling was favored over coherent rotation ranged from S = 1.05 for needle-like particles to S = 1.44 for spheres. Many other models and calculations have been reported, their reversal modes resembling modified fanning [*Knowles*, 1986; *Kuo*, 1988] or curling (vortex propagation) [*Schabes and Bertram*, 1988; *Uesaka et al.*, 1993].

[39] Our particles are quite elongate, with l/d = 14–40. For this range of axial ratios, S for the changeover between buckling or coherent rotation and curling is predicted to be 1.05–1.08. Given the inevitable variation in pore size in the Al_2O_3 film, it is conceivable that larger diameter particles curl while smaller ones buckle/fan. All three samples had the same basic pore size. The pores were left unwidened, while the iron electrodeposition time varied. Thus the only variable, apart from pore spacing, was particle length l. On the basis of the calculated S of 1.03 for 17-nm iron particles, sample 34, with l/d = 14 and a theoretical changeover S of 1.08, would be most likely to curl, while sample 96, with l/d = 40 and a critical S of 1.05, would be somewhat more likely to buckle. This is not the pattern observed (Figure 4) but it does suggest a possible reason why the experimental curves diverge when $\psi \geq 70°$.

[40] How relevant are our observations to the situation in nature? Magnetite rather than iron is the "typical" terrestrial magnetic mineral. S values and corresponding critical sizes scale upward by a factor of about 3.5 (the ratio of M_s values in the two materials). Critical sizes are 50–70 nm instead of 17 nm. Micromagnetic calculations predict that coherent rotation changes to curling/vortex reversal at about this diameter [*Enkin and Williams*, 1994; *Fabian et al.*, 1996; *Newell and Merrill*, 1999].

[41] Although these calculations are verified in a general way by the predictions they make about the changeover from SD (or flower) to vortex remanent states, direct experimental tests of the reversal mode have yet to be made. Measurable aligned arrays of particles might be found in individual crystals of plagioclase or clinopyroxene [*Renne et al.*, 2002; *Feinberg et al.*, 2005] or by aligning bacterial magnetosome chains in a strong field and setting or freezing them to make a sample. *Penninga et al.* [1995] were able to demonstrate that individual *Magnetospirillum magnetotacticum* bacteria have only two remanent states and switch between them at fields that vary from cell to cell but are almost constant with angle for $0 \leq \psi \leq 45°$, as for fanning or curling.

6. Conclusions

[42] Our attempts to establish experimental SD hysterons at 10° intervals of ψ, the angle between $\boldsymbol{H}$ and the easy axis, were frustrated by the imperfections of our samples: 6–8.5° average misalignment of particle axes (Figure 5), particle interactions that suppress the characteristic fanning peak in $H_c(\psi)$ (Figure 3), and a distribution of particle coercivities due to interactions, angular dispersion, and variations in particle size d and aspect ratio l/d. The misalignment problem is most vexing for large ψ, where loop shape changes rapidly. The measured ψ = 90° loop bears a closer resemblance to experimental and predicted loops for ψ = 80° than to the predicted ψ = 90° ramp (Figures 2d and 2e). The coercivity distribution is most evident at small angles, ψ = 0–30°, where it produces steep, but not vertical, irreversible arms of the hysteresis loop (Figures 2 and 2b). The best we can do for now is to adopt a set of theoretical hysterons for identical aligned particles, based on a combination of coherent rotation, fanning and curling in different ranges of ψ.

[43] Unlike *Salling et al.* [1994], who measured $H_{crit}(\psi)$ of individual ellipsoidal SD particles using Lorentz microscopy and found it to be compatible with coherent rotation over almost the entire range of ψ, our $H_{cr}(\psi)$ data (Figure 4) imply that only the initial reversible rotation of particle moments occurs coherently. Irreversible switching seems to occur by fanning for $\psi \leq 60°$ and either fanning or curling at higher angles. Our $H_{cr}(\psi)$ curves diverge above 60° and do not match the curling relation $(1 - \alpha\ \sin^2\psi)^{-1/2}$ (equation (3)) closely but they do resemble curves for fanning and curling rather than coherent rotation.

[44] The Day plot has been used to distinguish among minerals and to analyze quantitatively mixtures of SP, SD, PSD and MD grains of magnetite [*Dunlop*, 2002a, 2002b; *Dunlop and Carter-Stiglitz*, 2006]. According to Figure 6, M_{rs}/M_s and H_{cr}/H_c are also correlated in a distinctive way for assemblies of uniaxial SD grains with their easy axes aligned. Orientation of the applied field $\boldsymbol{H}$ determines position along the correlation curve, and conversely Day plot coordinates are an indicator of ψ, with an uncertainty of about ±5° from one sample to another.

[45] **Acknowledgments.** We are grateful to Song Xu and Özden Özdemir for their experimental assistance. Careful and helpful reviews by

Bruce Moskowitz and an anonymous referee improved the paper. This research has been supported by NSERC Canada through grant A7709 to D.J.D.

References

Aharoni, A. (1963), Complete eigenvalue spectrum for the nucleation in a ferromagnetic prolate spheroid, *Phys. Rev.*, *131*, 1478–1482.

Aharoni, A. (1966), Magnetization curling, *Phys. Status Solidi*, *16*, 1–41.

Aharoni, A. (1986), Angular dependence of nucleation field in magnetic recording particles, *IEEE Trans. Magn.*, *22*, 149–150.

Aharoni, A. (1997), Nucleation modes in ferromagnetic prolate spheroids, *J. Phys. Condens. Matter*, *9*, 10,009–10,021.

Aharoni, A., and S. Shtrikman (1958), Magnetization curve of the infinite cylinder, *Phys. Rev.*, *109*, 1522–1528.

AlMawlawi, D., N. Coombs, and M. Moskovits (1991), Magnetic properties of Fe deposited into anodic aluminum oxide pores as a function of particle size, *J. Appl. Phys.*, *70*, 4421–4425.

Bottoni, G. (1991), Influence of the magnetic interactions on the reversal mode of magnetic recording particles, *J. Appl. Phys.*, *69*, 4499–4501.

Brown , W. F., Jr. (1963), *Micromagnetics*, 143 pp., Wiley-Interscience, Hoboken, N. J.

Butler, R. F., and S. K. Banerjee (1975), Single-domain grain size limits for metallic iron, *J. Geophys. Res.*, *80*, 252–259.

Carvallo, C., D. J. Dunlop, and Ö. Özdemir (2005), Comparison of FORC and remanent Preisach diagrams, *Geophys. J. Int.*, *162*, 747–754.

Day, R., M. Fuller, and V. A. Schmidt (1977), Hysteresis properties of titanomagnetites: Grain size and composition dependence, *Phys. Earth Planet. Inter.*, *13*, 260–267.

Dunlop, D. J. (2002a), Theory and application of the Day plot (M_{rs}/M_s versus H_{cr}/H_c): 1. Theoretical curves and tests using titanomagnetite data, *J. Geophys. Res.*, *107*(B3), 2056, doi:10.1029/2001JB000486.

Dunlop, D. J. (2002b), Theory and application of the Day plot (M_{rs}/M_s versus H_{cr}/H_c): 2. Application to data for rocks, sediments, and soils, *J. Geophys. Res.*, *107*(B3), 2057, doi:10.1029/2001JB000487.

Dunlop, D. J., and B. Carter-Stiglitz (2006), Day plots of mixtures of superparamagnetic, single-domain, pseudo-single-domain and multidomain magnetites, *J. Geophys. Res.*, doi:10.1029/2006JB004499, in press.

Dunlop, D. J., and Ö. Özdemir (1997), *Rock Magnetism: Fundamentals and Frontiers*, 573 pp., Cambridge Univ. Press, New York.

Dunlop, D. J., S. Xu, Ö. Özdemir, D. AlMawlawi, and M. Moskovits (1993), Magnetic properties of arrays of oriented iron particles as a function of particle size, shape and spacing, *Phys. Earth Planet. Inter.*, *76*, 113–121.

Dunlop, D. J., Ö. Özdemir, and D. G. Rancourt (2006), Magnetism of biotite crystals, *Earth Planet. Sci. Lett.*, *243*, 805–819.

Egli, R., and W. Lowrie (2002), Anhysteretic remanent magnetization of fine magnetic particles, *J. Geophys. Res.*, *107*(B10), 2209, doi:10.1029/2001JB000671.

Enkin, R. J., and W. Williams (1994), Three-dimensional micromagnetic analysis of stability in fine magnetic grains, *J. Geophys. Res.*, *99*, 611–618.

Fabian, K., A. Kirchner, W. Williams, F. Heider, T. Leibl, and A. Hubert (1996), Three-dimensional micromagnetic calculations using FFT, *Geophys. J. Int.*, *124*, 89–104.

Feinberg, J. M., G. R. Scott, P. R. Renne, and H.-R. Wenk (2005), Exsolved magnetite inclusions in silicates: Features determining their remanence behavior, *Geology*, *33*, 513–516.

Fulmek, P. L., and H. Hauser (1994), Coercivity and switching field of single-domain γ-Fe_2O_3 particles under consideration of the demagnetizing field, *J. Appl. Phys.*, *76*, 6561–6563.

Furneaux, R. C., G. E. Thompson, and G. C. Wood (1978), The application of ultramicroscopy to the electronoptical examination of surface films on aluminum, *Corros. Sci.*, *18*, 853–881.

Hendriksen, P. V., G. Christiansen, and S. Mørup (1994), Magnetization reversal in chain-like clusters of interacting particles, *J. Magn. Magn. Mater.*, *132*, 207–218.

Jacobs, I. S., and C. P. Bean (1955), An approach to elongated fine particle magnets, *Phys. Rev.*, *100*, 1060–1067.

Kneller, E. F., and F. E. Luborsky (1963), Particle size dependence of coercivity and remanence of single-domain particles, *J. Appl. Phys.*, *34*, 656–658.

Knowles, J. E. (1986), Magnetization reversal by flipping in acicular particles of γFe_2O_3, *J. Magn. Magn. Mater.*, *61*, 121–128.

Knowles, J. E., R. F. Pearson, and A. D. Annis (1980), The angular distribution of the magnetization in magnetic recording tapes, *IEEE Trans. Magn.*, *16*, 42–44.

Kobayashi, A., et al. (2006), Experimental observation of magnetosome chain collapse in magnetotactic bacteria: Sedimentological, paleomagnetic, and evolutionary implications, *Earth Planet. Sci. Lett.*, *245*, 538–550.

Kuo, P. C. (1988), Chain-of-spheres calculation on the coercivities of elongated fine particle with both magnetocrystalline and shape anisotropy, *J. Appl. Phys.*, *64*, 5071–5083.

Lanci, L., and D. V. Kent (2003), Introduction of thermal activation in forward modeling of hysteresis loops for single-domain magnetic particles and implications for the interpretation of the Day diagram, *J. Geophys. Res.*, *108*(B3), 2142, doi:10.1029/2001JB000944.

Luborsky, F. E., and T. O. Paine (1960), Angular variation of the magnetic properties of elongated single-domain iron particles, *J. Appl. Phys.*, *31*, supplement, 66S–70S.

Luo, Y., and J.-G. Zhu (1994), Switching field characteristics of individual iron particles by MFM, *IEEE Trans. Magn.*, *30*, 4080–4082.

Néel, L. (1949), Théorie du traînage magnétique des ferromagnétiques en grains fins avec applications aux terres cuites, *Ann. Geophys.*, *5*, 99–136.

Newell, A. J., and R. T. Merrill (1999), Single-domain critical sizes for coercivity and remanence, *J. Geophys. Res.*, *104*, 617–628.

Newell, A. J., and R. T. Merrill (2000), Nucleation and stability of remanent states, *J. Geophys. Res.*, *105*, 19,377–19,391.

Penninga, I., H. de Waard, B. M. Moskowitz, D. A. Bazylinski, and R. B. Frankel (1995), Remanence measurements on individual magnetotactic bacteria using a pulsed magnetic field, *J. Magn. Magn. Mater.*, *149*, 279–286.

Pontifex, G. H., P. Zhang, Z. Wang, T. L. Haslett, D. AlMawlawi, and M. Moskovits (1991), STM imaging of the surface of small metal particles formed in anodic oxide pores, *J. Phys. Chem.*, *95*, 9989–9993.

Preisach, F. (1935), Über die magnetische Nachwirkung, *Z. Phys.*, *94*, 277–302.

Renne, P. R., G. R. Scott, J. M. G. Glen, and J. M. Feinberg (2002), Oriented inclusions of magnetite in clinopyroxene: Source of stable remanent magnetization in gabbros of the Messum Complex, Namibia, *Geochem. Geophys. Geosyst.*, *3*(12), 1079, doi:10.1029/2002GC000319.

Salling, C., R. O'Barr, I. McFadyen, and M. Ozaki (1994), Investigation of the magnetization reversal mode for individual ellipsoidal single-domain particles of γ-Fe_2O_3, *J. Appl. Phys.*, *75*, 7989–7992.

Schabes, M. E., and H. N. Bertram (1988), Ferromagnetic switching in elongated γ-Fe_2O_3 particles, *J. Appl. Phys.*, *64*, 5832–5834.

Stephenson, A., and J. C. Shao (1994), The angular dependence of the median destructive field of magnetite particles, *Geophys. J. Int.*, *118*, 181–184.

Stoner, E. C., and E. P. Wohlfarth (1948), A mechanism of magnetic hysteresis in heterogeneous alloys, *Philos. Trans. R. Soc. London, Ser. A*, *240*, 599–642.

Uesaka, Y., Y. Nakatani, and N. Hayashi (1993), Computer simulations of switching fields and magnetization reversal mechanisms of interacting cubic particles: Cases with fields applied parallel to the easy axis, *J. Magn. Magn. Mater.*, *123*, 209–218.

Williams, W., and D. J. Dunlop (1995), Simulation of magnetic hysteresis in pseudo-single-domain grains of magnetite, *J. Geophys. Res.*, *100*, 3859–3871.

D. J. Dunlop, Geophysics, Department of Physics, University of Toronto, Toronto, ON, Canada M5S 1A7. (dunlop@physics.utoronto.ca)

G. A. Milne, Department of Earth Sciences, University of Durham, Durham DH1 3LE, UK.